Monthly Notices of the ROYAL ASTRONOMICAL SOCIETY

MNRAS **510,** 1375–1382 (2022) https://doi.org/10.1093/mnras/stab3433
Advance Access publication 2021 November 27

Internally driven warps in disc galaxies

J. A. Sellwood[1]★ and Victor P. Debattista[2]★

[1]*Steward Observatory, University of Arizona, 933 N Cherry Ave, Tucson, AZ 85722, USA*
[2]*Jeremiah Horrocks Institute, University of Central Lancashire, Preston PR1 2HE, UK*

Accepted 2021 November 22. Received 2021 October 25; in original form 2021 September 17

ABSTRACT

Any perturbation to a disc galaxy that creates a misalignment between the planes of the inner and outer disc, will excite a slowly evolving bending wave in the outer disc. The torque from the stiff inner disc drives a retrograde, leading spiral bending wave that grows in amplitude as it propagates outwards over a period of several Gyr. The part of the disc left behind by the outwardly propagating wave is brought into alignment with the inner disc. This behaviour creates warps that obey the rules established from observations, and operates no matter what the original cause of the misalignment between the inner and outer disc. Here, we confirm that mild warps in simulations of disc galaxies can be excited by shot noise in the halo, as was recently reported. We show that the quadrupole component of the noise creates disc distortions most effectively. Bending waves caused by shot noise in carefully constructed equilibrium simulations of isolated galaxies are far too mild to be observable, but perturbations from halo substructure and galaxy assembly must excite larger amplitude bending waves in real galaxies.

Key words: galaxies: evolution – galaxies: kinematics and dynamics – galaxies: spiral – galaxies: structure.

1 INTRODUCTION

Warps in the neutral hydrogen layer of the Milky Way (e.g. Oort, Kerr & Westerhout 1958; Levine, Blitz & Heiles 2006) and other disc galaxies (e.g. Sancisi 1976; Bosma 1991) are now established as a common feature of galaxies. The visible disc can also be twisted to a smaller extent; where both are observed, the distortion of the stellar layer may follow that of the gas in some galaxies, e.g. UGC 7170 (Cox et al. 1996), which is strong evidence that its warp is a gravitationally driven phenomenon. Shen & Sellwood (2006) successfully modelled the 'prodigious' warp of NGC 4013 as a gravitationally driven bending wave. However, there are also galaxies, e.g. NGC 4565 (Radburn-Smith et al. 2014) and perhaps also the Milky Way (Reylé et al. 2009; Chen et al. 2019), that have a second type of warp in which the gas, and even some young stars, are outside the stellar layer defined by the old disc. The more likely explanation for the misaligned gas and young stars in these cases is off-axis gas accretion. Our focus in this paper is on warps of the first kind.

Briggs (1990) identified three rules that were followed by all the well-observed galaxies in his sample:

(i) The H I layer typically is coplanar inside radius R_{25}, the radius where the B-band surface brightness is 25 mag arcsec^{-2}, and the warp develops between R_{25} and $R_{26.5}$ (the Holmberg radius).
(ii) The line of nodes (LoN) is roughly straight inside $R_{26.5}$.
(iii) The LoN takes the form of a loosely wound leading spiral outside $R_{26.5}$.

Kahn & Woltjer (1959) first drew attention to the theoretical challenge presented by disc warps, emphasizing that the gravitational stresses in a twisted disc would be too weak to resist the winding of the warp by differential precession. As the theory of gravitationally driven warps was thoroughly reviewed by Sellwood (2013), we here briefly summarize two aspects that are of relevance to this paper.

1.1 Bending waves in discs

The frequency of bending waves of wavenumber, $k = 2\pi/\lambda$, in a uniform, razor-thin, sheet of stars having a mass surface density Σ is given by the dispersion relation

$$\omega^2 = 2\pi G\Sigma|k| - \sigma_x^2 k^2 + \nu_{\rm ext}^2, \tag{1}$$

where σ_x is the stellar velocity dispersion in the direction of the wave, i.e. perpendicular to the wave crests, and $\nu_{\rm ext}^2 = |\partial^2\Phi_{\rm ext}/\partial z^2|_{z=0}$ (Binney & Tremaine 2008) is the squared vertical oscillation frequency due to mass, such as the bulge and halo, that is not in the sheet. Bending waves are stable when $\omega^2 > 0$, which requires $\lambda > \sigma_x^2/G\Sigma$ if $\nu_{\rm ext} = 0$.

The WKB approximation assumes equation (1) holds for tightly wrapped bending waves in a thin disc, which requires wavelengths short enough that their curvature can be neglected, or ideally that $|kR| \gg 1$. As for spiral waves, the tight winding approximation allows one to write the forcing frequency $\omega = m(\Omega_{\rm p} - \Omega_{\rm c})$ for an m-armed bending wave. Here, $\Omega_{\rm p}$ is the angular pattern speed of the wave and $\Omega_{\rm c}$ is the local circular frequency. Even though bending waves in real galaxies are not short-wavelength tightly wrapped disturbances, this analysis is believed to give some qualitative indication of their behaviour. With these approximations, the group velocity of a packet of bending waves is (Toomre 1983)

$$v_{\rm g} \equiv \frac{\partial\omega}{\partial k} = \frac{{\rm sgn}(k)\pi G\Sigma - k\sigma_{\rm R}^2}{m(\Omega_{\rm p} - \Omega_{\rm c})}. \tag{2}$$

The convention adopted in this analysis is that $k < 0$ for leading waves, and therefore the group velocity of slow ($\Omega_{\rm p} \ll \Omega_{\rm c}$) leading

★ E-mail: sellwood@email.arizona.edu (JAS); vpdebattista@gmail.com (VPD)

waves is positive, or radially outward in the disc. Note that an outwardly decreasing surface density of the disc has two consequences: first, v_g slows as a wave packet moves outward and secondly, by analogy with whips, wave action conservation requires its amplitude also to rise.

1.2 Warps

Hunter & Toomre (1969) studied the bending modes of isolated, razor-thin discs with no random motion. They found that the Maclaurin disc, which has a sharp outer edge, had a discrete spectrum of bending modes, but only two trivial modes existed in discs that had fuzzy edges: a uniform vertical displacement and a simple tilt of the entire disc. The importance of a fuzzy edge is that bending waves travel ever more slowly as they approach the edge and could never reflect to create the standing wave required for a mode. Although this conclusion holds only for discs lacking random motion (see Sellwood 1996, for a counter-example), the effect of galaxy haloes has gradually emerged as a greater obstacle to the idea that warps could be long-lived modes of discs.

Sparke & Casertano (1988) developed an idea originally due to Dekel & Shlosman (1983) that galactic warps arise because the disc of a galaxy is misaligned with the principal plane of a rigid oblate (or prolate) dark matter halo. The twist of the disc, which they described as a modified tilt mode, arose where the dominant contribution to the gravitational field transitioned from the disc to the misaligned halo. Unfortunately, their assumption that the halo would behave as a rigid mass distribution does not hold; Kuijken & Dubinski (1995), Binney, Jiang & Dutta (1998), and Shen & Sellwood (2006) all reported that the orbits of live halo particles quickly adjust to the total potential of the disc plus halo to eliminate the hypothesized misalignment.

The most promising idea for warp creation originated with Ostriker & Binney (1989), who proposed that the angular momentum of late infalling material as a disc galaxy is assembled would probably be misaligned with the angular momentum vector of the original disc. This idea was explored by Quinn & Binney (1992), and the gravitational attraction of a misaligned annulus of matter was modelled by Jiang & Binney (1999) and Shen & Sellwood (2006). These last authors, in particular, reported antisymmetric ($m = 1$) bending waves in the disc that would last not forever, but for long enough that it is likely that any galaxy would suffer further accretion of material having a different angular momentum vector before the first warp had decayed.

Alternatively the gas warp is the infalling material itself. In massive galaxies, gas is believed to reach the disc via hot accretion, in which the intergalactic gas is shock-heated as it crosses the halo's virial radius (e.g. Fall & Efstathiou 1980; Brook et al. 2004; Kereš et al. 2005; Robertson et al. 2006). Cosmological simulations show that the angular momentum of the resulting hot gas corona is randomly oriented with respect to that of the disc (van den Bosch et al. 2002; Velliscig et al. 2002; Stevens et al. 2017; Obreja et al. 2019). Consequently, cooling coronal gas reaches the disc misaligned, forming a warp (Roškar et al. 2010), which also drives a slow tilting of the disc (Earp et al. 2019). This picture naturally explains why gaseous warps are traced only by younger stars in the Milky Way (Chen et al. 2019) and NGC 4565 (Radburn-Smith et al. 2014).

1.3 Present study

With this background, Chequers & Widrow (2017, hereafter CW17) were surprised to find long-lived coherent bending waves in their two stellar dynamical simulations of isolated Milky Way models. Here, we create and evolve similar simulations which show that CW17 correctly attributed the excitation of disc distortions to particle noise in the halo. We also show that these disturbances created coherent gravitationally driven bending waves in the disc that are easily understood.

The mechanism for the slowly evolving warps that we, and earlier Shen & Sellwood (2006), identify is quite general and requires only that the inner disc be misaligned with the outer disc, no matter what created the misalignment.

2 TECHNIQUE

2.1 Disc–bulge–halo model

We adopt the model for a disc galaxy embedded in a bulge and halo that was previously used by Sellwood (2021). The dense bulge inhibits bar instabilities (Toomre 1981), and the disc supports mild spirals.

(i) The exponential disc has the surface density

$$\Sigma(R) = \frac{M_\mathrm{d}}{2\pi R_\mathrm{d}^2} \exp(-R/R_\mathrm{d}), \tag{3}$$

where M_d is the mass of the notional infinite disc and R_d is the disc scale length. The vertical density profile of the disc is Gaussian with a scale $0.1R_\mathrm{d}$ and, in this work, we truncate the disc at $7R_\mathrm{d}$. Since we are interested in warps in the outer disc, employing equal mass particles to represent such an extensive disc would result in merely $\sim$1 per cent of the disc particles in the range $6 < R/R_\mathrm{d} < 7$. In order to employ a larger fraction of the particles in the outer disc, we set the masses of the particles $\propto R \exp(-R/R_\mathrm{d})/R_\mathrm{d}$, based on their initial radii, to achieve equal numbers in equal radial bins while preserving the exponential density profile (3).

(ii) We use a dense Plummer sphere for the bulge, which has a mass of $0.1M_\mathrm{d}$ and core radius $a = 0.1R_\mathrm{d}$, and adopt the isotropic distribution function (DF) given by Dejonghe (1987). The bulge is dense enough that it dominates the central attraction in the inner part of our model, and the analytic DF is close to equilibrium despite the presence of the disc and halo.

(iii) We start from a Hernquist (1990) model for the halo that has the density profile

$$\rho(r) = \frac{M_\mathrm{h} b}{2\pi r(b+r)^3}, \tag{4}$$

where M_h is the total mass integrated to infinity and b is a length-scale. We choose $M_\mathrm{h} = 5M_\mathrm{d}$ and $b = 4R_\mathrm{d}$. Naturally, the isotropic DF that Hernquist derived for this isolated mass distribution would not be in equilibrium when the disc and bulge are added, so we use the adiabatic compression procedure described by Sellwood & McGaugh (2005) that starts from the DF given by Hernquist and uses the invariance of both the radial and azimuthal actions to compute a revised density profile and DF as extra mass is inserted. The revised DF has a slight radial bias but remains spherical. We also apply an outer cut-off to the selected particles that excludes any with enough energy ever to reach $r > 10b$, which causes the halo density to taper smoothly to zero at that radius.

The resulting rotation curve of the model is illustrated in Fig. 1, where we have scaled the model, both here and throughout the paper, so that $R_\mathrm{d} = 3$ kpc and the unit of time $(R_\mathrm{d}^3/GM_\mathrm{d})^{1/2} = 12$ Myr, which implies a disc mass $M_\mathrm{d} = 4.17 \times 10^{10}\,\mathrm{M}_\odot$.

We adopt a constant value of $Q = 1.5$ at all radii to determine the radial velocity dispersion of the disc particles. Although the disc is

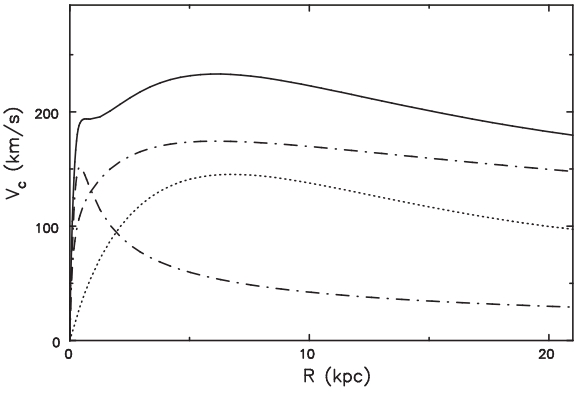

Figure 1. The initial rotation curve of our galaxy model (solid curve) measured from the particles. The disc contributes the dotted line, while the dot–dashed lines indicate the contributions of the bulge and compressed halo.

Table 1. Default numerical parameters.

Polar grid size	$175 \times 256 \times 125$
Grid scaling	$R_\mathrm{d} = 10$ grid units
Vertical spacing	$\delta z = 0.02 R_\mathrm{d}$
Active sectoral harmonics	$0 \le m \le 4$
Softening length	$R_\mathrm{d}/10$
Spherical grid	501 shells
Active spherical harmonics	$0 \le l \le 4$
Number of disc particles	10^7
Number of halo particles	10^7
Number of bulge particles	10^6
Basic time-step	$(R_\mathrm{d}^3/GM)^{1/2}/320$
Time-step zones	6

quite massive, the high value of the epicyclic frequency, κ, near the centre in particular implies random velocities are modest everywhere, and the Jeans equations in the epicyclic approximation (Binney & Tremaine 2008) yield an excellent disc equilibrium.

2.2 Numerical method

The particles in our simulations move in a 3D volume that is spanned by two separate grids; a cylindrical polar mesh and a much larger spherical grid. The self-gravitational attractions are calculated at grid points and interpolated to the position of each particle. The disc particles are initially assigned to the polar grid, while the spherical grid is used for the bulge and halo particles. Naturally, all particles are attracted by all others at every step. A full description of our numerical procedures is given in the on-line manual (Sellwood 2014) and the code itself is available for download.

Table 1 gives the default values of the numerical parameters for the simulations presented in this paper, and cases where they are changed are noted in the text. It is easy to restrict the spherical harmonics that contribute to the field of the halo particles. Also, the sectoral harmonics that contribute to the field of the disc particles on a polar grid, since that part of the gravitational field is a convolution of the mass density with a Green function that is most efficiently computed by Fourier transforms.

2.3 Other details

We define a set of radii $\{R_k\}$ that are spaced every $0.2R_\mathrm{d}$ to separate the disc into radial bins and measure bending distortions in each bin

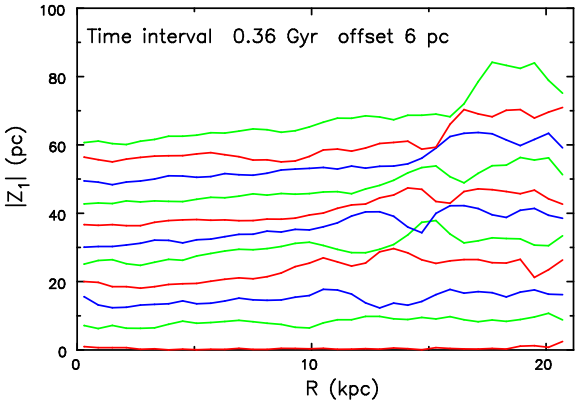

Figure 2. The radial variation of $|Z_1|$ at equal time intervals in our standard run. Successive lines, which are drawn at intervals of 0.36 Gyr, are shifted upward by 6pc and are coloured to make them easier to trace, and values based on fewer than 1000 particles are skipped. This integral sign warp reaches a peak amplitude of ∼24 pc near the outer edge of the disc by the last moment shown measured at $t = 3.6$ Gyr, which is the 11th line.

by forming the transform

$$Z_m(R_{k+n}, t) = \frac{\sum_j w_n \mu_j z_j \mathrm{e}^{im\phi_j}}{\sum_j w_n \mu_j}, \qquad n = 0, 1 \tag{5}$$

where μ_j is the mass and $(R_j,\ \phi_j,\ z_j)$ are the cylindrical polar coordinates of the jth particle at time t. The weights w_0 and w_1 share the particle's contribution linearly according to its radius R_j between the rings at R_k and R_{k+1}.

In order to measure frequencies of m-fold symmetric bending waves that we assume have coherent frequencies across a broad swath of the disc, we fit these data using the procedure described by Sellwood & Athanassoula (1986). Here, we assume constant amplitude waves that are the real part of

$$\mathcal{Z}_m(R_k, \phi, t) = \mathcal{A}_m(R_k)\mathrm{e}^{i(m\phi - \omega t)}, \tag{6}$$

where the frequency $\omega = m\Omega_\mathrm{p}$ and Ω_p is the pattern speed. We will be concerned exclusively with $m = 1$ warps, and generally we fit for two co-existing coherent waves. The complex function for each disturbance $\mathcal{A}_m(R_k)$, which is independent of time, describes the radial variation of the vertical displacement and phase of the wave, which would be a normal mode of the system if $\mathcal{A}_m(R_k)$ is strictly independent of time for all $\{R_k\}$, or it may simply be a bending wave propagating slowly across the disc. It is possible to fit for growing displacements by allowing ω to be complex, but we do not do that here.

3 RESULTS

Our first result, presented in Fig. 2, reveals qualitatively similar behaviour to that reported by CW17, although there are significant quantitative differences. The salient feature is that a small warp develops spontaneously, as CW17 reported, even though the disc is almost completely stable to in-plane disturbances and no external perturbations are applied. By the last moment shown, at 3.2 Gyr, the warp near the outer disc edge reaches an amplitude of $\gtrsim 20$ pc over the radial range $17 < R < 20$ kpc, whereas CW17 reported that the warps in their models reached an amplitude of ∼100 pc by 4 Gyr and 300–400 pc by 10 Gyr. CW17 suggested that their warps propagated outwards across the disc, and there is a hint from Fig. 2 that may also happen in our model. Note also that the $|Z_1|$ displacements in the

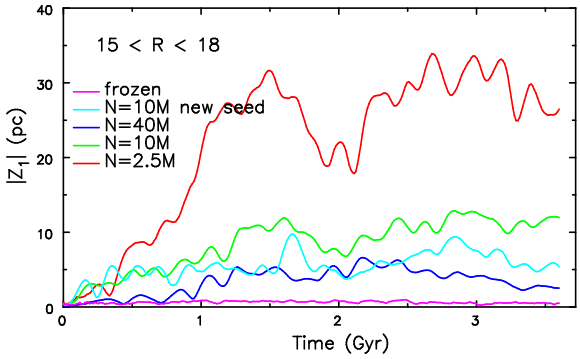

Figure 3. The time evolution of the mass-weighted average of $|Z_1|$ over the radial range given in kpc in five simulations. The green line is from our standard case (Fig. 2), for which $N_{\rm halo} = 10$M, and the numbers of particles employed in each mass component was reduced (red) and increased (blue) by factor of 4. The magenta line shows the effect of freezing the halo and bulge, while we simply changed the random seed in our standard run to obtain the result shown by the cyan line.

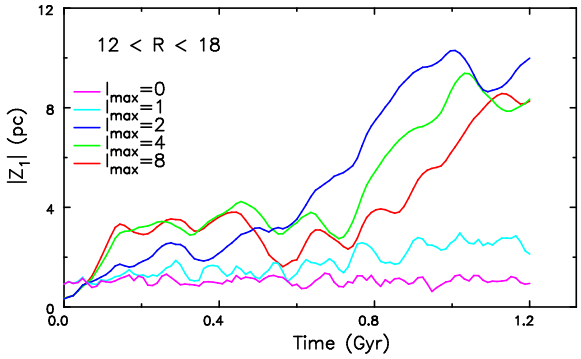

Figure 4. As for Fig. 3, the early evolution of five simulations identical with our standard run, but in which we varied the order of expansion when determining the gravitational field of the halo and bulge particles. The Z_m values were averaged over the given radial range in kpc. Again the green line is from our standard case (Fig. 2), for which $l_{\rm max} = 4$.

inner part of the disc in Fig. 2 have a tendency to rise almost linearly, suggesting that the inner disc could be tilting rigidly, as we confirm later, while the outer disc seems to flap less coherently.

Our model has a different bulge and halo from either of the models used by CW17; we employed four times as many particles for the disc and bulge and twice the number of halo particles, and we have used a grid-based code whereas they used a tree code. Also the $|Z_1|$ displacements reported in Fig. 2 are relative to the original disc plane of our model, whereas the warps reported by CW17 were relative to the plane of the inner disc.

The warp in Fig. 2 is of smaller amplitude than that reported by CW17 for two reasons: first, they compute the evolution of their models for approximately three times as long, during which time the amplitude in the outer disc continued to increase and, secondly, we employed more particles. When we employed one quarter the number of particles in each component, we found that the warp amplitude reached $\sim$100 pc by 3.6 Gyr in reasonable agreement with their value at 4 Gyr. Furthermore, we recomputed the same initial file of particles of our smaller N model using a tree code (PKDGRAV; Stadel 2001) with a softening length of 50 pc, finding a good quantitative agreement to $t = 4$ Gyr with the results from the grid code, and also with CW17.

3.1 Excitation mechanism

We both reduced and increased the numbers of particles in each mass component by factors of four, to obtain the red and blue curves shown in Fig. 3, which reveal that the warp amplitude, which fluctuates a great deal with time, generally seems to decrease with increasing N. Note that the warp amplitudes reported in this figure are mass-weighted averages over the indicated radial range. Freezing the halo prevents any warp from developing (magenta line), and changing the initial random seed (cyan line) leads to quite different evolution. This evidence indicates that the warp is excited by shot noise from the halo particles, which is reduced by increasing N, eliminated by freezing the halo, and is subject to stochastic variations as the noise spectrum is changed by a new random seed.

Fig. 4 presents the effect on the disc warp of changing the number of spherical harmonics used to compute forces from the halo and bulge particles; note these are shorter runs and the vertical scale differs from that in Fig. 3. Again our standard case, with $l_{\rm max} = 4$, is shown by the green line, but increasing the order of expansion to $l_{\rm max} = 8$ (red line) made only a small difference. The warp behaviour was little different from that in a frozen halo when we eliminated all aspherical terms (magenta line), although in this case the halo particles were moving, and therefore the monopole terms would have been subject to shot noise fluctuations. The dipole term (cyan line) excites a very mild warp, but the quadrupole term ($l = 2$) is clearly dominant (blue line), and the warp grows more rapidly when $l_{\rm max} = 2$ than it does when higher multipoles are included. It should also be noted that we tried filtering out the $l = 1$ and $l = 3$ terms, while retaining $l = 0$, 2, and 4, obtaining a result that was virtually indistinguishable from the green curve for which the odd-l terms were included.

The evidence in Fig. 4 is that the dominant component that excites the warp is the quadrupole term in the expansion for the gravitational field of the halo. This seems physically reasonable, since a quadrupole field that is misaligned with the plane of the disc will attract the disc upward on one side and downward on the other, exciting an $m = 1$ warp in the disc.

The torque from shot noise acting on the disc is feeble and changes in both amplitude and direction with time as the halo particles move on their orbits. Some density fluctuations excite the warp and, presumably, others damp it, so the warp amplitude evolution is partly a random walk caused by the evolving changes in the halo that apply a changing torque on the disc. Stochastic variations in the torque acting on the disc must be partly responsible for the non-smooth time variation of the bending amplitude (Fig. 3).

To investigate this more fully, we divided the halo in our standard run into 10 energy bins, each containing 1M particles, and computed a spherical harmonic expansion, to $l_{\rm max} = 4$, of the density distribution in each shell. Tightly bound particles have the shortest orbit periods and the direction of the quadrupole measured in the innermost shells changes rapidly. But we found some temporal coherence in the orientation of the quadrupole in higher E bins, albeit with considerable jitter. Fig. 5 shows the orientation of the quadrupole in the 6th energy bin, averaged over the time intervals tabulated on the right.

The initial orientation in this energy bin, black symbol, lies near $\phi \simeq 190^\circ$ with $\theta \simeq 32^\circ$, suggesting that the halo attracts the disc upward near this value of ϕ. Because the disc is rotating, the first tilt of the disc plane should be in the direction given by the vector cross product of the disc angular momentum and the applied torque, which is approximately true as shown in Fig. 6. The radial range

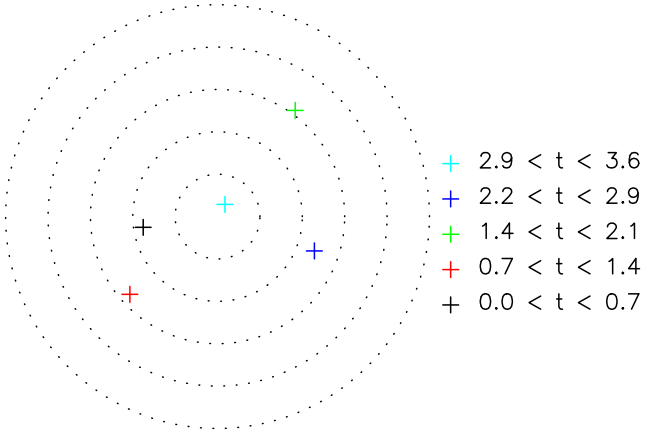

Figure 5. The time evolution of the halo quadrupole orientation, (ϕ, θ), estimated from the particles in the sixth energy bin of the halo that have a mean radius of ∼15 kpc. Each coloured point shows the average orientation during the period in Gyr indicated in the right margin. Polar angles are relative to the stationary simulation frame; the radial coordinate is θ with the centre being on the symmetry axis, $\theta = 0$, and the outermost circle, $\theta = \pi/2$, is in the mid-plane, while the azimuth is ϕ. Only the upper hemisphere is shown, as the quadrupole has two-fold symmetry.

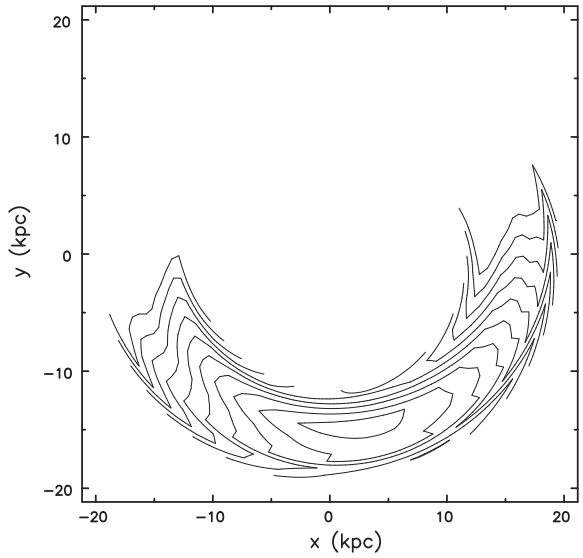

Figure 6. The tilt of an annulus of the disc averaged over the interval from the start to 0.72 Gyr, in response to the torque from the black symbol in Fig. 5, which was computed from a similar radial range. Only positive Z_1 displacements are shown. Note that the disc tilt is approximately at right angles to the applied torque, as required by the vector cross product, since the disc rotates counter-clockwise in this projection.

shown in the disc was chosen to match that of the halo particles used to compute the torque orientation in Fig. 5, while the time interval corresponds to that shown by the black symbol.

3.2 Properties of the warp

The initial forcing of the disc by the weak halo torques tilt the plane of the disc as a rigid body in the inner parts, where the high surface density and random motion make the inner disc stiff (e.g. Debattista & Sellwood 1999; Shen & Sellwood 2006). These stiffening factors weaken with radius, and the outer disc from $R \gtrsim 4R_d$ (Shen &

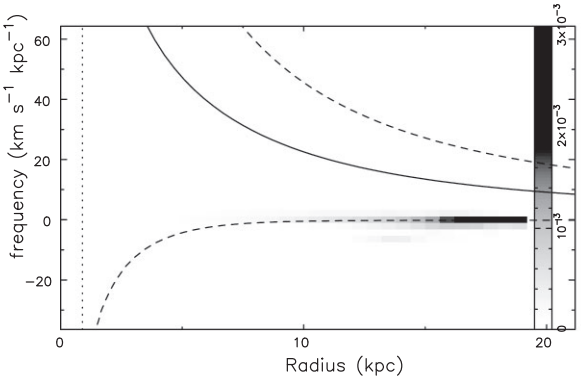

Figure 7. A spectrum showing power in the Z_1 distortions of the disc as functions of frequency and radius in our standard simulation. The time interval extends over almost the entire evolution, and the radial range excludes the centre (inside the dotted line) and the outer edge of the disc (where the grey-scale begins). The solid curve marks the radial variation of the circular frequency Ω_c, and the dashed curves $\Omega_c \pm \nu_{ext}$, with ν_{ext} being the vertical oscillation frequency caused by the attraction of the bulge and halo, i.e. neglecting the self-force of the disc.

Sellwood 2006) is not constrained to tip with the massive inner disc. These statements are supported by the evidence in Fig. 2. As soon as the outer disc becomes misaligned with the inner, the dominant torque on it is no longer from the weak noise torques of the nearby halo, but the coherent torque from the misaligned inner disc. This strong torque causes the outer disc to precess in the retrograde direction (Shen & Sellwood 2006; Sellwood 2013), while the massive inner disc barely moves in response to the mild back reaction from the light outer disc.

All parts of the disc continue to be subject to torques from the halo noise which must cause the inner disc tilt to change slowly, but the dominant behaviour remains a barely moving inner disc that drives a retrograde precession of the outer disc. This behaviour is confirmed by the power spectrum of the Z_1 distortions in the disc over almost the entire evolution of our standard model in Fig. 7. It reveals an almost zero frequency disturbance over most of the disc, together with a retrograde disturbance near the outer edge. The frequencies of self-gravitating warps are expected to be farther from corotation than $\Omega_c \pm \nu_{ext}$, and the slow wave to have a retrograde pattern speed (Sellwood 2013). Here, ν_{ext} is the vertical frequency determined by the attraction of the bulge and halo, neglecting that of the disc, as defined in Section 1.1.[1]

We have used the fitting code of Sellwood & Athanassoula (1986) to reveal the nature of these two disturbances and display the results in Fig. 8. The top panel shows that the disturbance of near zero frequency is indeed a simple tilt of the disc, as hinted in Fig. 2, whereas the retrograde disturbance has a leading spiral shape, as also expected for slow warp waves (Section 1.1). We have not seen any evidence for exponential growth, and so regard the warp as a driven response, not an instability. We find that the orientation of the inner disc tilt does change very slowly over time, and that shown in top panel of Fig. 8, which is drawn at the last fitted moment, differs from that shown at the much earlier time in Fig. 6.

We made similar fits to the data from the models of different N, fitting two neutrally stable modes over $1.2 < t < 3.6$ Gyr. In each

[1]The locations of warp resonances in a thickened disc depend on ν_{ext} only, and not the total vertical frequency $\nu = (\nu_{ext}^2 + \nu_{int}^2)^{1/2}$ as was incorrectly stated by Sellwood (2013, section 8.1).

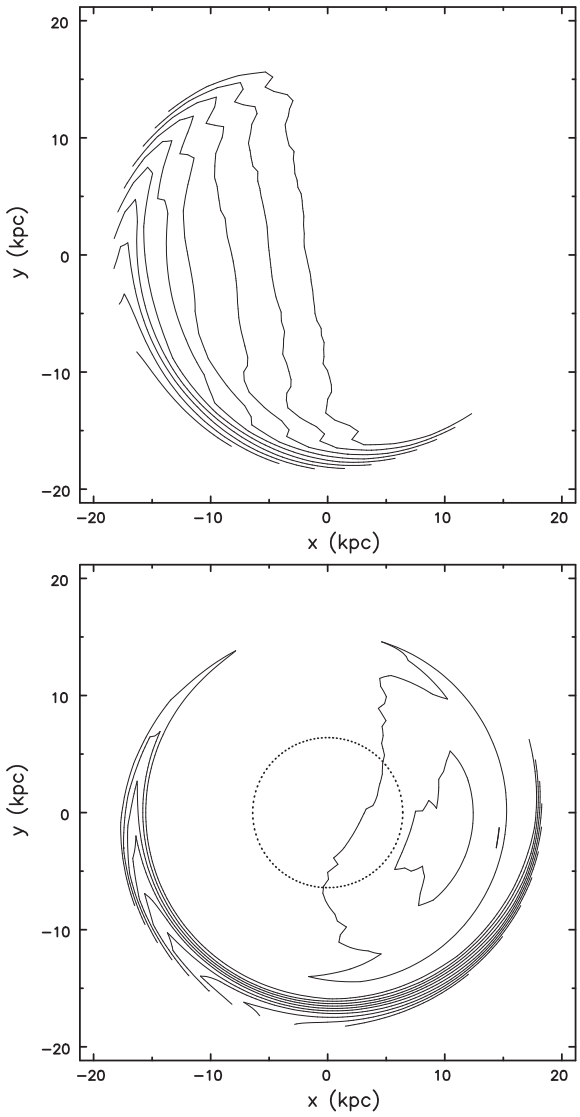

Figure 8. The two best-fitting disturbances to the Z_1 displacement data from our standard model. The fit picks out time averages of the Z_1 displacement amplitude of possibly steadily rotating waves over the interval from 1.2 to 3.6 Gyr, and only positive Z_1 displacements are shown. The dotted circle marks the radius at which $\Omega_p = \Omega_c - \nu_{ext}$ for the retrograde rotating wave.

case, the fitted disturbances look very similar to those in Fig. 8, and the frequencies are almost the same, although the amplitudes differ, as expected.

We do not suggest the leading spiral is a real mode, but rather a time average of a slowly evolving response driven by the misaligned inner disc. The group velocity of a leading bending wave is radially outward (equation 2); not only does it slow as the disc surface density decreases, but action conservation requires its amplitude also to rise.

3.3 A further test

In order to confirm that the later evolution of the warp is largely driven by disc dynamics, and is less affected by the stochastic torque from the halo, we recomputed the later evolution of our standard run (Fig. 2) in a frozen halo. After 0.72 Gyr, when the inner disc had been tilted by the halo torque, we replaced the live halo and bulge by

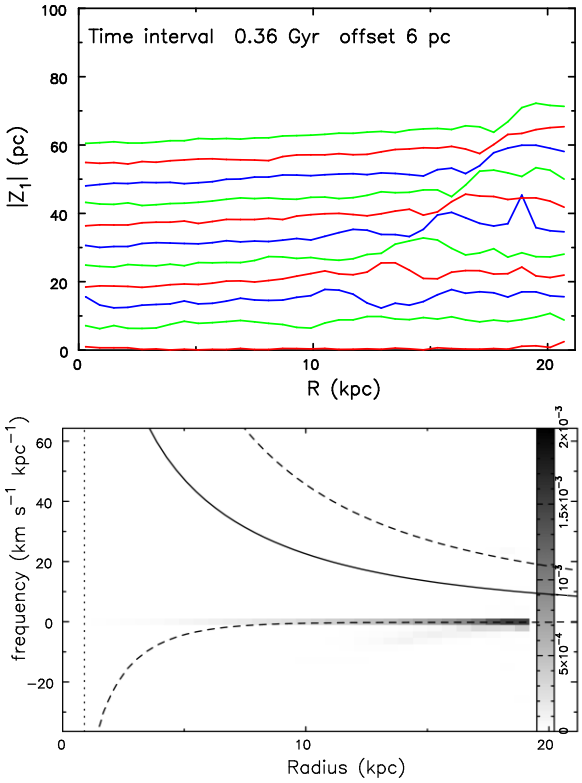

Figure 9. Upper: As for Fig 2, which was drawn for our standard run, but for the new case in which the halo was frozen after 0.72 Gyr. Although the warp is smaller, both the uniform tilt of the inner disc and the outward propagation of the bending wave are much clearer. Lower: The power spectrum of $m = 1$ distortions in the new run with the frozen halo over the same time interval as shown in for the live halo in Fig. 7.

rigid, smooth spherical mass distributions having the same density profiles so that the disc equilibrium was unaffected.

The time evolution of the warp in the new late-frozen halo case is shown in the upper panel of Fig. 9, which is to be compared with our standard result in Fig. 2. The first three lines, at $t = 0$, 0.36, and 0.72 Gyr are identical, of course, but the later amplitude of the warp is lower in the frozen halo case and fluctuates less – presumably because the disc is no longer being jerked around by on-going halo noise. Note that both the uniform tilt of the inner disc and the outward propagation of the bending wave are much clearer in Fig. 9 than in Fig. 2, and the radial extent of the uniformly tilted disc grows as the bending wave propagates outward. The power spectrum from the late-frozen run is shown in the lower panel, which again reveals a near stationary disturbance and a faint retrograde wave in the outer disc. These were the principal features in the comparison case with the live halo (Fig. 7), but the retrograde wave is less pronounced in the late-frozen case.

The two fitted waves in Fig. 10 also closely resemble those in Fig. 8, with the leading spiral shape being somewhat clearer in the lower panel of Fig. 10. This difference, and the different orientations of the two disturbances, presumably arise because the inner disc is not subject to on-going halo noise in the late-frozen case.

This behaviour when the bulge and halo are rigid, smooth, spheres confirms that the outwardly propagating wave in the outer disc can be driven only by the torque from the inner disc.

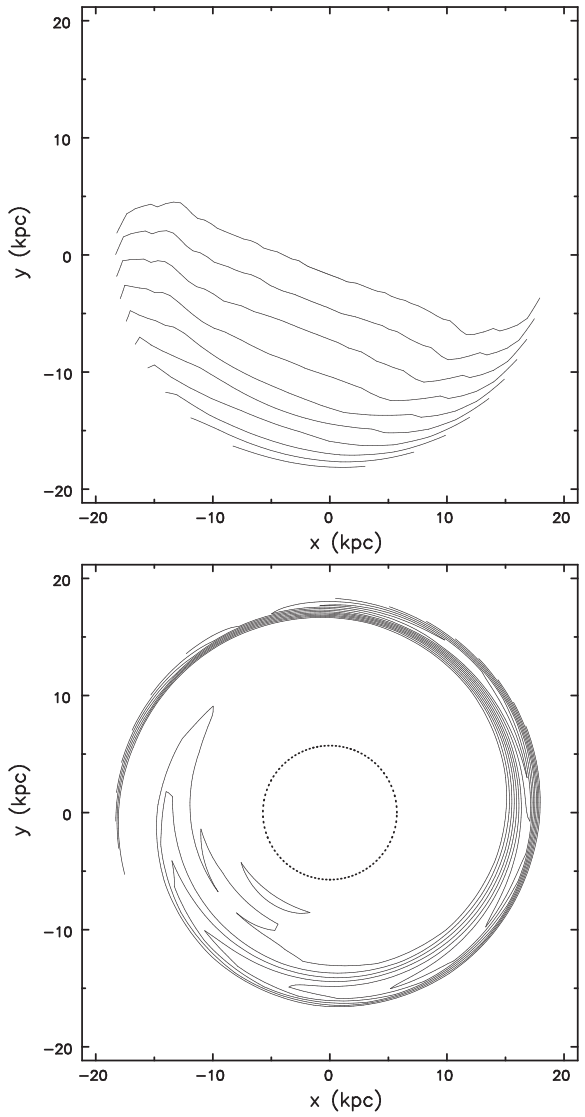

Figure 10. The two best-fitting disturbances to the Z_1 displacement data from the late-frozen model, to be compared with the similar fit over the same time interval in our standard run with the live halo in Fig. 8.

4 CONCLUSIONS

Our principal conclusion is that a misalignment between the inner and outer disc drives an outwardly propagating bending wave that grows in amplitude through action conservation and persists for several Gyr. As the wave propagates outwards, it brings the previously misaligned outer disc into alignment with the inner disc. This behaviour, which was also reported by Shen & Sellwood (2006), does not depend on the cause of the misalignment or on its amplitude – their simulation revealed a much larger warp that behaved in exactly the same way as the mild features we report here.

The disc is a flywheel with a huge store of angular momentum, and the inner part is quite stiff. The inner disc therefore responds to any externally applied torque by tipping slightly, while the outer part may tip more. As soon as a misalignment between the inner and outer disc is established, it launches an outwardly travelling, retrograde, leading spiral bending wave. We showed here that this behaviour persisted in a case in which we froze the halo after some evolution, demonstrating that the dynamical mechanism is indeed dominated by the misalignment between the inner and outer disc.

We have confirmed the result from CW17 that mild warps are excited stochastically by halo noise. The supporting evidence is that we find warp amplitudes decrease in experiments having larger numbers of halo particles, which have milder density fluctuations, and changing the random seed leads to a completely different warp history. We have developed this picture by showing that the warp is excited most effectively by the quadrupole component of the halo noise. Since the quadrupole can have any orientation, which will generally be inclined to disc plane, it naturally excites an $m = 1$ tip to the disc.

All the warps reported in this paper are excited by the very mild shot noise in our carefully constructed equilibrium halo, and such small warps would be barely observable. Halo substructure in real galaxies, on the other hand, as well as any residual sloshing motions from galaxy assembly, will exert larger perturbing forces that would also be more temporally coherent as the sub-haloes move on their orbits.

ACKNOWLEDGEMENTS

JAS acknowledges the continuing hospitality of Steward Observatory. VPD is supported by STFC consolidated grant no. ST/R000786/1.

DATA AVAILABILITY

The data from the simulations reported here can be made available on request. The simulation code can be downloaded from http://www.physics.rutgers.edu/galaxy

REFERENCES

Binney J., Tremaine S., 2008, Galactic Dynamics, 2nd edn. Princeton Univ. Press, Princeton, NJ
Binney J., Jiang I.-G., Dutta S., 1998, MNRAS, 297, 1237
Bosma A., 1991, in Casertano S., Sackett P. D., Briggs F. H., eds, Warped Disks and Inclined Rings Around Galaxies. Cambridge Univ. Press, Cambridge, p. 181
Briggs F. H., 1990, ApJ, 352, 15
Brook C. B., Kawata D., Gibson B. K., Freeman K. C., 2004, ApJ, 612, 894
Chen X., Wang S., Deng L., de Grijs R., Liu C., Tian H., 2019, Nat. Astron., 3, 320
Chequers M. H., Widrow L. M., 2017, MNRAS, 472, 2751(CW17)
Cox A. L., Sparke L. S., van Moorsel G., Shaw M., 1996, AJ, 111, 1505
Debattista V. P., Sellwood J. A., 1999, ApJ, 513, L107
Dejonghe H., 1987, MNRAS, 224, 13
Dekel A., Shlosman I., 1983, in Athanassoula E., ed., Proc. IAU Symp. 100, Internal Kinematics and Dynamics of Galaxies. Reidel, Dordrecht, p. 187
Earp S. W. F., Debattista V. P., Macciò A. V., Wang L., Buck T., Khachaturyants T., 2019, MNRAS, 488, 5728
Fall S. M., Efstathiou G., 1980, MNRAS, 193, 189
Hernquist L., 1990, ApJ, 356, 359
Hunter C., Toomre A., 1969, ApJ, 155, 747
Jiang I.-G., Binney J., 1999, MNRAS, 303, L7
Kahn F. D., Woltjer L., 1959, ApJ, 130, 705
Kereš D., Katz N., Weinberg D. H., Davé R., 2005, MNRAS, 363, 2
Kuijken K., Dubinski J., 1995, MNRAS, 277, 1341
Levine E. S., Blitz L., Heiles C., 2006, ApJ, 643, 881
Obreja A. et al., 2019, MNRAS, 487, 4424
Oort J. H., Kerr F. J., Westerhout G., 1958, MNRAS, 118, 379
Ostriker E. C., Binney J. J., 1989, MNRAS, 237, 785
Quinn T., Binney J., 1992, MNRAS, 255, 729

Radburn-Smith D. J. et al., 2014, ApJ, 780, 105
Reylé C., Marshall D. J., Robin A. C., Schultheisé M., 2009, A&A, 495, 819
Robertson B., Bullock J. S., Cox T. J., Di Matteo T., Hernquist L., Springel V., Yoshida N., 2006, ApJ, 645, 986
Roškar R., Debattista V. P., Brooks A. M., Quinn T. R., Brook C. B., Governato F., Dalcanton J. J., Wadsley J., 2010, MNRAS, 408, 783
Sancisi R., 1976, A&A, 53, 159
Sellwood J. A., 1996, ApJ, 473, 733
Sellwood J. A., 2013, in Oswalt T. D., Gilmore G., eds, Planets Stars and Stellar Systems, Vol. 5. Springer, Heidelberg, p. 923
Sellwood J. A., 2014, preprint (arXiv:1406.6606)
Sellwood J. A., 2021, MNRAS, 506, 3018
Sellwood J. A., Athanassoula E., 1986, MNRAS, 221, 195
Sellwood J. A., McGaugh S. S., 2005, ApJ, 634, 70
Shen J., Sellwood J. A., 2006, MNRAS, 370, 2
Sparke L. S., Casertano S., 1988, MNRAS, 234, 873
Stadel J. G., 2001, PhD thesis, Univ. Washington
Stevens A. R. H., Lagos C. del P., Contreras S., Croton D. J., Padilla N. D., Schaller M., Schaye J., Theuns T., 2017, MNRAS, 467, 2066
Toomre A., 1981, in Fall S. M., Lynden-Bell D., eds, The Structure and Evolution of Normal Galaxies. Cambridge Univ. Press, Cambridge, p. 111
Toomre A., 1983, in Athanassoula E., ed., Proc. IAU Symp. 100, Internal Kinematics and Dynamics of Galaxies. Reidel, Dordrecht, p. 177
van den Bosch F. C., Abel T., Croft R. A. C., Hernquist L., White S. D. M., 2002, ApJ, 576, 21
Velliscig M. et al., 2015, MNRAS, 453, 721

This paper has been typeset from a TEX/LATEX file prepared by the author.